

# BLADE MOTION CORRELATION FOR THE FULL-SCALE UH-60A AIRLOADS ROTOR

**Ethan Romander**  
ethan.romander@nasa.gov

**Larry Meyn**  
larry.meyn@nasa.gov

**Thomas R. Norman**  
tom.norman@nasa.gov

Aeromechanics Office; NASA Ames Research Center; Moffett Field, CA

**Danny Barrows**  
danny.a.barrows@nasa.gov  
Advanced Sensing and Optical  
Measurement Branch  
NASA Langley Research Center  
Hampton, VA

**Alpheus Burner**  
alpheus.w.burner@nasa.gov  
Jacobs Technology  
Hampton, VA

## ABSTRACT

A recently completed wind tunnel test of a full-scale UH-60A rotor included multiple measurements of blade motion. Pitch, flap, and lag hinge rotations were captured by a mechanical “crabarm” as well as a system of laser distance transducers. In addition, a novel technique utilized photogrammetry to track the motion of 48 targets arrayed on the bottom of each blade. The photogrammetry technique is capable of quantifying blade deformation in addition to hinge rotations. These measurements are compared to a coupled Computational Fluid Dynamics / Comprehensive Rotorcraft Analysis simulation. Correlation between measurement and simulation is generally very good, resulting in maximum deviations on the order of a few degrees. Pitch bearing motion suggests that small inaccuracies in the aerodynamic analysis are leading to a slightly different trim state than the measured data. A consistent mean shift for lag motion indicates a deficiency in the structural dynamics model. Comparisons of flap motion as well as flap bending and torsion are also presented and correlate within the expected error bands.

## NOTATION

<p><math>a_\infty</math> freestream speed of sound</p> <p><math>A</math> total rotor disk area, <math>\pi R^2=2262 \text{ ft}^2</math></p> <p><math>c</math> local chord length</p> <p><math>C_P</math> rotor power coefficient, <math>\frac{P}{\rho(\Omega R)^3 A}</math></p> <p><math>C_T</math> rotor thrust coefficient, <math>\frac{T}{\rho(\Omega R)^2 A}</math></p> <p><math>C_X</math> rotor propulsive force coefficient, <math>\frac{X}{\rho(\Omega R)^2 A}</math></p> <p><math>f_n</math> force perpendicular to local chord line</p> <p><math>m</math> moment about local quarter chord</p> <p><math>M^2_{c_n}</math> sectional normal force coefficient, <math>\frac{df_n/dr}{1/2\rho a_\infty^2 c}</math></p> <p><math>M^2_{c_m}</math> sectional pitching coefficient, <math>\frac{dm/dr}{1/2\rho a_\infty^2 c^2}</math></p> <p><math>M_{tip}</math> tip Mach number</p>	<p><math>N</math> number of blades, 4</p> <p><math>P</math> total rotor power</p> <p><math>R</math> rotor radius, 26.83 ft</p> <p><math>T</math> rotor thrust</p> <p><math>V_\infty</math> freestream velocity</p> <p><math>X</math> rotor propulsive force</p> <p><math>\alpha_c</math> wall corrected shaft angle</p> <p><math>\theta_{.75}</math> collective angle, deg</p> <p><math>\mu</math> advance ratio, <math>\frac{V_\infty}{\Omega R}</math></p> <p><math>\rho</math> freestream density</p> <p><math>\sigma</math> rotor solidity, <math>\frac{N \cdot \bar{c}}{\pi R} = 0.0826</math></p> <p><math>\psi</math> rotor azimuth, deg</p> <p><math>\Omega</math> rotor angular velocity, rad/sec</p>
---	--

---

Presented at the Fifth Decennial AHS Aeromechanics Specialists’ Conference; San Francisco, CA; January 22–24, 2014. This is a work of the U.S. Government and is not subject to copyright protection in the United States.

## INTRODUCTION

The UH-60 Airloads Test Program has a history that spans more than 20 years. The goal of this joint Army/NASA program is to provide a complete set of high-quality measurements that could be used to refine state-of-the-art analytic methods. The first data were acquired on a scale model rotor in the Duits Netherlands Wind Tunnel (DNW) in Holland in 1989 [1]. Four years later, a full-scale Airloads flight test was conducted [2]. The latest dataset produced by this test program was completed in May 2010 in the USAF’s National Full-Scale Aerodynamics Complex (NFAC) 40- by 80-Foot Wind Tunnel [3]. It is data from this most recent test that is featured in the present paper.

The 2010 wind tunnel test acquired data over a wide range of test conditions [3], including speed sweeps at 1-g simulated flight conditions and parametric thrust sweeps (up to and including stall) at various combinations of shaft angle and forward speed. These conditions included airspeeds up to 175 kt and thrusts up to 32,000 lb. Data were also acquired at matching conditions from the previous full-scale flight test and small-scale DNW wind tunnel test to assess rotor and wind tunnel scaling issues. Finally, unique slowed-rotor data were acquired at reduced RPM (40% and 65%), achieving advance ratios up to 1.0.

The rotor used for the 2010 test was the same test article used during the 1993 flight test. Figure 1 shows this rotor mounted on the NFAC Large Rotor Test Apparatus (LRTA) in the wind tunnel test section. The LRTA balance provided rotor performance data while the blades themselves were instrumented to acquire surface pressures and blade loads. The hub was equipped to provide measurements of blade motion. Rotor wake measurements were made using large-field Particle Image Velocimetry (PIV) and Retro-reflective Background-Oriented Schlieren techniques. Rounding out this dataset was a series of blade motion measurements taken using a non-intrusive photogrammetric technique.

Attempts have been made to correlate many of these measurements with simulations. These include Romander [4], Lee-Rausch [5], and Potsdam [6] who have correlated against blade airloads and rotor performance measurements. Yeo [7] provided the initial comparison with blade structural loads measurements. Ahmad [8] has compared analysis with PIV wake measurement data. The blade motion measurements received a brief comparison with simulation in an introductory paper by Abrego [9]. The purpose of this paper is to expand upon that effort in more depth while considering additional



Figure 1 – UH-60A airloads rotor in NFAC 40- by 80-Foot Wind Tunnel.

test conditions.

## BLADE MOTION MEASUREMENT

Three independent systems were used to measure blade motion during the 2010 Airloads Test. The first was a purely mechanical system utilizing rotary transducers and a “crabarm” affixed to each blade to provide measurements of pitch, flap, and lag motion for each blade. This system also flew on the 1993 flight test and is commonly referred to as the Blade Motion Hardware (BMH). Some components of the BMH system are shown in Fig. 2. A second system used a trio of laser distance transducers affixed to each hub arm to provide redundant measurements of pitch, flap, and lag motion for each blade. Elements of the laser system are also visible in Fig. 2. Complete descriptions of these measurement systems are found in [3]. The final blade motion measurement system, called the blade displacement (BD) system, is based on the principles of close-range photogrammetry [9].

The core of the BD measurement system was a series of cameras with high-powered azimuthally synchronized strobes installed in the wind tunnel floor and an array of 48 retroreflective targets affixed to the bottom of each blade (see Fig. 3). Image sets were acquired with the rotor in motion during testing. Post-processing involved feeding these images through a data processing pipeline to identify targets in the images and cross-correlate their locations between cameras. This located the targets in three dimensional space. Further processing compared the target locations to a reference geometry in order to deduce not only blade pitch, flap, and lag but also elastic deformation along the blade.

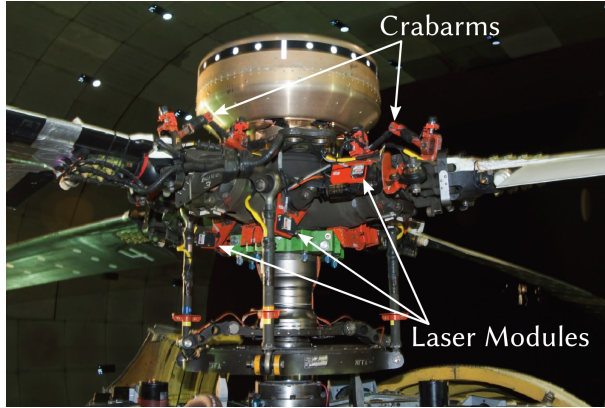


**Figure 2** – Blade Motion Hardware (crabarms) and laser modules.

BD image sets were categorized as either primary or secondary. Primary datasets consisted of 60 revolutions of data for each blade at each of 40 azimuthal locations around the whole rotor disk. Secondary datasets acquired just 12 revolutions of data at 11 azimuthal locations for each blade in its own, separate quadrant. Secondary datasets therefore require that data from all four blades be combined to obtain a full revolution of motion data. Abrego [9] noted blade-to-blade differences in excess of  $1^\circ$  of pitch, flap, and lag motion for some test conditions. These blade-to-blade differences would manifest as discontinuities at quadrant boundaries for secondary datasets. For this reason, it was decided to only correlate against primary datasets for the present paper.

The data from all of these measurement systems are still considered preliminary. The BMH and laser systems provide measurements that generally agree well. The mean components of the BMH measurements are believed to be more reliable than those of the laser system and so no results from the laser system will be presented in this paper. However, even the BMH measurements exhibit differences from one blade to another. 128 revolutions of data acquired at each test condition were first averaged together to yield a single average time history for each blade. Then blades with unreliable data were eliminated based on engineering judgment and the remaining data were averaged to provide a single BMH time history for each test condition. Primary BD datasets contain 240 (60 revolutions for each of 4 blades) separate measurements at each of the 40 azimuthal locations. For this paper, the 60 samples for each blade were first averaged together at each azimuth and then the data for the four blades were averaged to provide a mean time history of blade motion around the azimuth.

## SIMULATION METHODOLOGY

The complexity of rotorcraft aeromechanics is not easily modeled. The analytical results presented herein were obtained using two separate codes—each a specialist in a particular aspect of rotorcraft simulation—collaborating for this purpose. This section will describe the two codes and how they work together to maximize simulation accuracy and efficiency.

### OVERFLOW 2

All Navier-Stokes CFD analyses presented herein were performed using OVERFLOW 2 version 2.2e [10]. OVERFLOW 2 is an overset, structured-mesh flow solver developed at NASA. For two decades the OVERFLOW solver has served to analyze a variety of rotorcraft under a wide range of flight conditions [11]. OVERFLOW 2 offers a wide variety of numerical schemes, turbulence models, and boundary conditions. For the present study, OVERFLOW 2 was run with 6<sup>th</sup> order central differencing and 4<sup>th</sup> order artificial dissipation in space. Time marching was performed using a 2<sup>nd</sup> order dual time-stepping scheme. Turbulence was modeled using the Spalart-Almaras one-equation model with rotational corrections and delayed detached eddy simulation [12]. Blade surfaces were treated as viscous, adiabatic walls. Outer boundaries were modeled using a characteristic condition imposing freestream quantities equivalent to a rotor operating in free air.

OVERFLOW 2 computes the flowfield by discretizing the Navier-Stokes equations on a series of overset, structured grids. Grids modeling the rotor blades were body-fitted and curvilinear. These grids, called near-body grids, extended approximately one chord length from the blade surface. The near-body grids were nested within a series of grids, called off-body grids, which filled the space between the rotor and the boundary of the computational domain. The OVERFLOW 2 model included a notional hub, but the LRTA and wind tunnel walls were not modeled. All grids exchanged flow information in regions of overlap. The amount of this overlap was sufficient to support full 6<sup>th</sup> order accuracy at the boundaries.

The blade surface grids can be logically divided into two portions at  $r/R=17\%$ . Outboard of this location the surface is derived from the as-built CAD model and is geometrically identical to grids used previously [4]. Inboard of this location the surface is a notional shank model developed from informal measurements and pictures of the actual test blade. The near-body grid representing the bulk of each rotor blade had an “O” topology

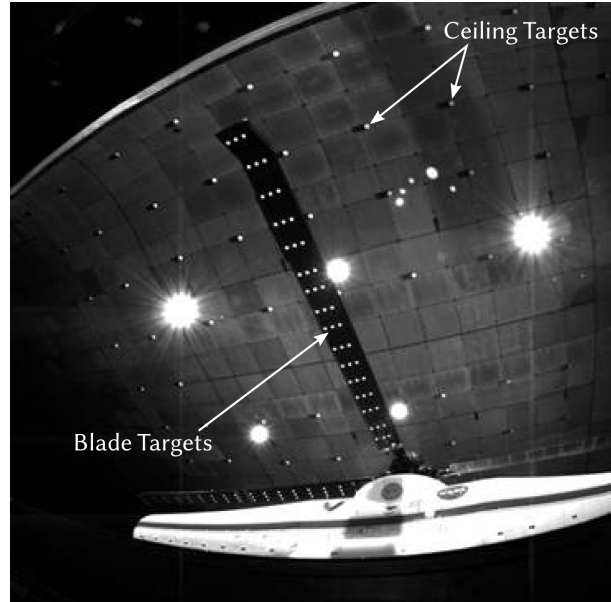
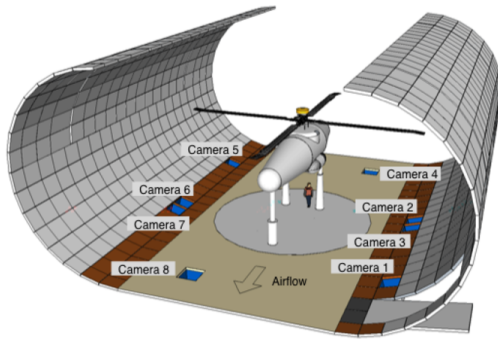


**Figure 3** – Blade Displacement measurement system with sample image.

with 241 points wrapping around the blade chordwise, 251 points along the blade span, and 75 points normal to the surface. The initial spacing normal to the blade surface had a  $y^+$  value of 1. This grid system is illustrated in Fig. 4. The near-body grid system (the hub and all four blades) contained approximately 27.1 million points.

The off-body grid system used a series of Cartesian grids to create shells expanding outward from the near-body grid set. The grid point spacing within each shell is twice that of the shell immediately preceding it. The finest off-body grid had a spacing equivalent to 0.1 tip-chord lengths in all three directions. Seven such shells created a cuboid computational domain spanning ten rotor radii in every direction. This off-body grid set consisted of 14.2 million grid points and is depicted in Fig. 5.

In total, this grid system contains approximately 41.3 million grid points. To reduce computation time CFD simulations were run using a hybrid distributed/shared memory scheme with 260 Message Passing Interface (distributed memory) ranks and four OpenMP threads (shared memory) per MPI rank for a total of 1040 parallel tasks. OVERFLOW 2 required approximately 60 minutes to advance the solution for this configuration  $\frac{1}{4}$  of a rotor revolution using 1040 CPUs of an SGI Altix ICE computer.

## CAMRAD II

CAMRAD II belongs to a family of software known as “Comprehensive Rotorcraft Analysis” (CRA) codes for the modeling of rotorcraft. These analyses incorporate a myriad of models to simulate the different aerodynamic and mechanical subsystems of a rotorcraft. CAMRAD II brings together a multibody dynamics model, a nonlinear finite element structural model, and an aerodynamics model based on lifting line theory [13]. The rotor is trimmed using Newton-Raphson iteration on collective and cyclic to meet specified trim targets. CAMRAD II has been used extensively in the simulation of the UH-60 aircraft in a variety of flight conditions [7, 14–18]. This study utilized CAMRAD II version 4.9.

The CAMRAD II structural dynamics model for the UH-60A has been decades in development by NASA and the U.S. Army. The baseline model was standardized in 2004 [14]. This model simulates the rotor using 7 1-D structural beam elements and 20 aerodynamic panels. However, this configuration is insufficient for coupled simulation wherein airloads must be communicated with high resolution in order to insure force conservation. Thus, the baseline model was modified to include 100 aerodynamic panels extending the full span of the OVERFLOW blade grid. Furthermore, the twist and chord distributions were modified to exactly match the corresponding values in the OVERFLOW grid. Finally, CAMRAD was configured to take  $1^\circ$  time-steps so that it made full use of the available temporal resolution

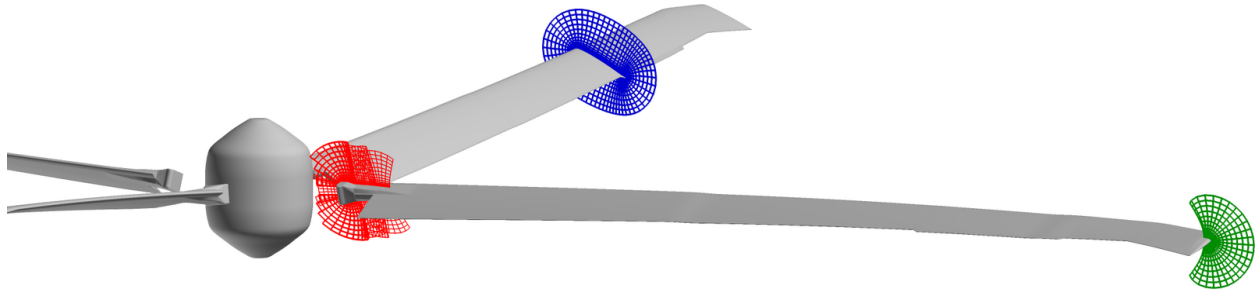


**Figure 4** – OVERFLOW 2 near-body grid system. (Not every point shown.)

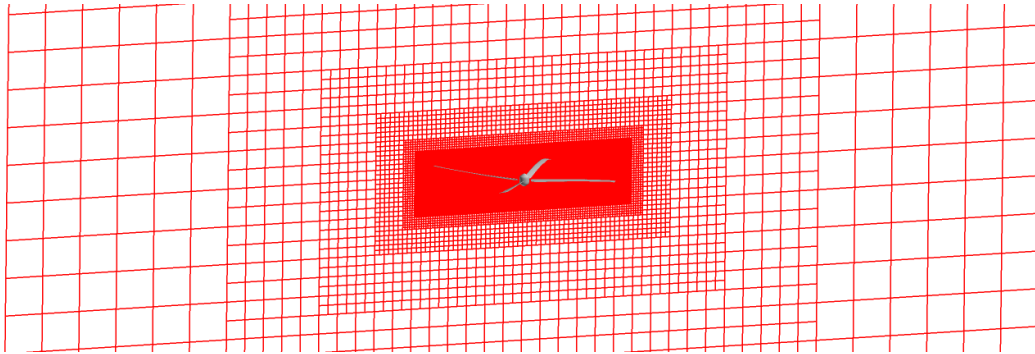


**Figure 5** – OVERFLOW 2 off-body grid system.

provided by OVERFLOW.

## COUPLING METHODOLOGY

CAMRAD II uses a lower-fidelity aerodynamics model than that available in modern CFD codes, and most CFD codes lack the sophisticated Computational Structural Dynamics and trim capabilities of comprehensive codes like CAMRAD II. Coupling a CFD code (e.g. OVERFLOW 2) to a comprehensive code (e.g. CAMRAD II) marries the strengths of the two approaches and produces the highest-fidelity solution currently possible. For this study, coupling is achieved by alternate execution of OVERFLOW 2 and CAMRAD II. At the end of each code's turn to execute it passes data to the next code. The data passed from OVERFLOW 2 to CAMRAD II is airload data integrated from its Navier-Stokes model of the UH-60 rotor. This airload data is used to augment CAMRAD II's internal aerodynamics model (which consists of airfoil tables and a lower-order wake model). At the end of its execution, CAMRAD II generates updated control positions and a description of how the blade deforms elastically as it revolves around the shaft. These quantities are used to give the OVERFLOW 2 grids a realistic motion in response to the aerodynamic environment. This algorithm, called the delta coupling technique, was pioneered by Tung [19] and

implemented in OVERFLOW by Potsdam [20]. Significantly improved airloads prediction capability has been demonstrated for the UH-60A rotor in steady level flight conditions using this loosely coupled approach [20, 21].

The CFD solution is advanced  $\frac{1}{4}$  revolution during a coupling iteration to allow each of the rotor's four blades to sweep through a full quadrant of the rotor disk. Taken in aggregate, the four blades thereby determine the airloads at every azimuth for every coupling iteration.

Convergence of the coupling process was determined by monitoring blade airloads for periodicity. When the airloads did not vary significantly from one coupling iteration to the next, the solution was judged to be converged. For the present analysis, this occurred within 24 coupling iterations. Since OVERFLOW 2 was allowed to iterate for  $\frac{1}{4}$  revolution between coupling exchanges, this equates to 6 full revolutions for the converged solution. A fully converged coupled solution required approximately 26 hours to compute for the baseline grid on 1040 SGI Altix ICE processors.

## SELECTED TEST CONDITIONS

Primary BD data is available for 28 different test conditions. From these, four were chosen for considera-

**Table 1** – Selected test conditions.

Run	Point	$\mu$	$M_{\text{tip}}$	$\alpha_c$	Collective Trim	Cyclic Trim
38	19	0.15	0.65	0.8	$C_T/\sigma=0.08$	Prescribed Moments
53	20	0.37	0.65	-8.0	$C_T/\sigma=0.08$	Prescribed Moments
42	46	0.24	0.65	1.6	$C_T/\sigma=0.13$	Minimum Moments
87	37	0.60	0.42	0.0	$\theta_{.75}=0$	Minimum Flapping

tion in this paper with preference given to conditions at the edge of the rotor’s operating envelope. All test conditions were simulated with a fixed shaft angle derived from the measured value by applying an appropriate wall correction [22]. Simulation collective and cyclic were trimmed to match measured thrust as well as roll and pitch moments. Except where noted, the rotor was operating at its nominal tip Mach number of 0.65. The four selected test conditions are summarized in Table 1.

The first test conditions are run 38, point 19 (3819) and run 53, point 20 (5320). Both are 1-G level flight states with  $C_T/\sigma=0.08$ . During the test, the shaft angle and cyclic were set to provide a propulsive force and hub moments representative of the UH-60 aircraft in these states. The difference between these two conditions is that 5320 is near the maximum speed of the UH-60 aircraft with  $\mu=0.37$  while 3819 is at a much slower  $\mu=0.15$ . At the lower advance ratio, the rotor experiences significant blade-vortex interactions on both the advancing and retreating sides.

Next was run 42, point 46 (4246). This condition placed the rotor in a deeply stalled state at its extreme thrust limit of  $C_T/\sigma=0.13$ . The advance ratio was a moderate 0.24, the geometric shaft angle was fixed at  $0^\circ$ , and the cyclic was trimmed to minimize hub moments.

Lastly run 87, point 37 (8737) was chosen from a pool of slowed-rotor test conditions unique to this test and designed to explore rotor performance at very high advance ratios. In particular, this point was at  $M_{\text{tip}} = 0.42$  (65% nominal), providing for an advance ratio of  $\mu=0.6$ . The geometric shaft angle and collective were both fixed at  $0^\circ$ . Cyclic was set to minimize  $1/\text{rev}$  flapping.

## RESULTS

This section will correlate selected simulation results with their corresponding test measurements. It will begin with a brief presentation of rotor performance and aerodynamics before concluding with a thorough discussion of blade motion.

## ROTOR AERODYNAMICS

Perfectly correlated blade motions are meaningless if the simulation failed to achieve parity with the test aerodynamic environment. Discussion of simulation accuracy relative to aerodynamic data from the Airloads Program generally centers on accurate prediction of blade sectional airloads. Three sectional forces—force normal to the chord line, force parallel to the chord line, and pitching moment about the quarter chord—are integrated from blade surface pressure data acquired during the Airloads Test. These same quantities can be similarly extracted from CFD computed aerodynamics. Figure 6 presents representative normal force and pitching moment at  $r/R=0.92$  for each of the selected test conditions. Chord force comparisons are not presented because limitations of the measurement artificially inflate the differences [5]. The level of correlation is generally similar to that observed in other research [4-6].

The low-speed case (3819) includes two blade-vortex interactions that cause large swings in the normal force—and to a lesser extent, pitching moment—on the advancing side near  $\psi=60^\circ$  and on the retreating side near  $\psi=270^\circ$ . Normal force for this case is generally very well predicted. Two clear exceptions are the overpredicted minima in the first and second quadrant. Calculated pitching moment slightly underpredicts the mean value. The rise in pitching moment from the second through the third quadrant is also not completely captured by the simulation.

Both pitching moment and normal force are well matched at the high-speed case (5320). The simulation displays a tendency to underpredict normal force on the advancing side paired with a tendency toward overprediction on the retreating side. Notably the negative lift peak on the advancing side is significantly overpredicted. Pitching moment is generally underpredicted on the retreating side although very well matched on the advancing side. A small impulse in the pitching moment near  $\psi=80^\circ$  is associated with supercritical flow and is accurately represented in the simulation.

For the high-thrust case (4246) the normal force predictions appear to lead the measured data by approxi-

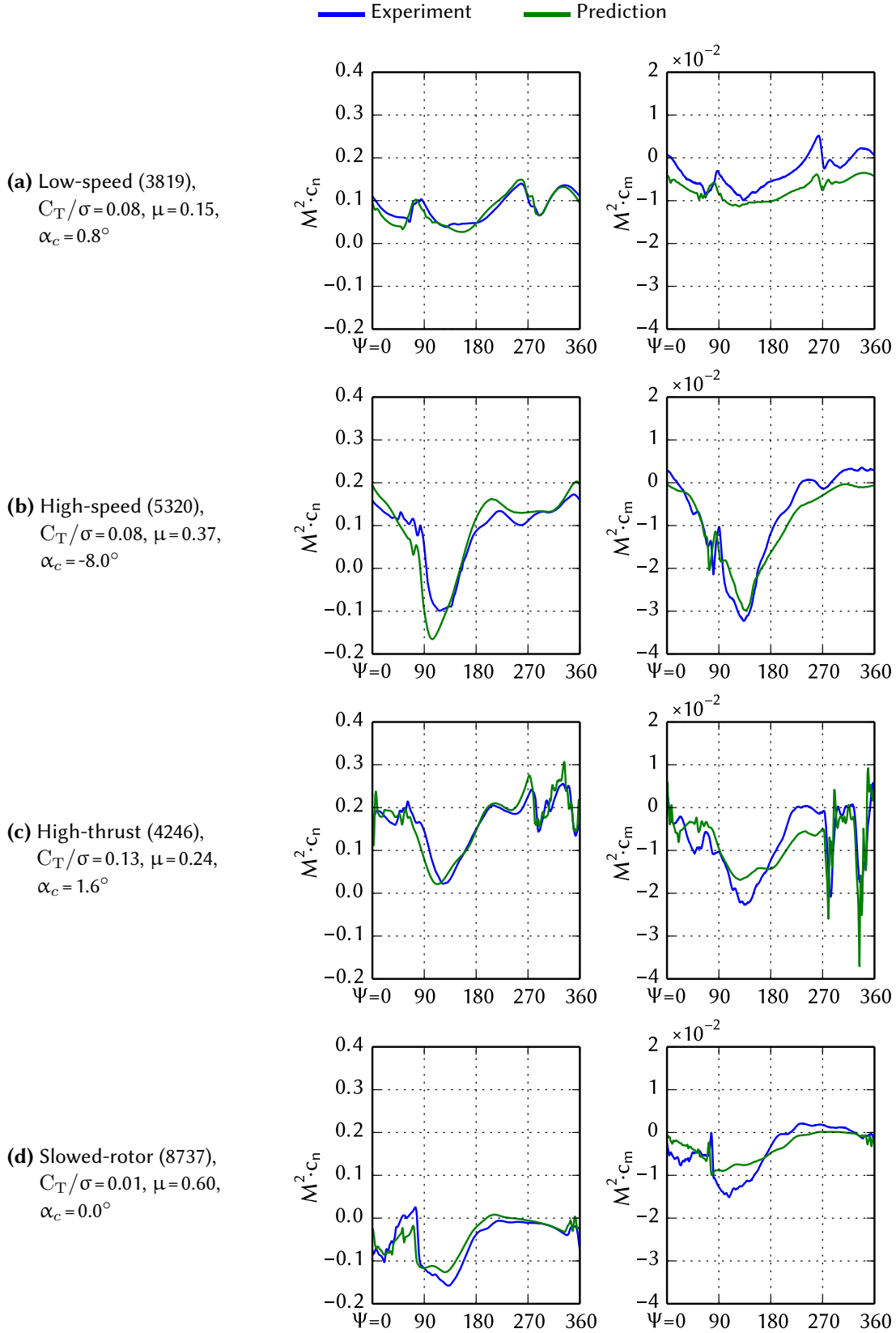


**Figure 6** – Sectional airloads at  $r/R=0.92$  for selected test conditions.

**Table 2** – Rotor performance correlation.

Test Condition	$C_P/\sigma$ ( $10^{-3}$ )			$C_X/\sigma$ ( $10^{-3}$ )		
	Measured	Predicted	Error	Measured	Predicted	Error
Low-speed	3.6	3.5	-0.12	1.2	0.59	-0.63
High-speed	8.5	8.7	0.21	9.6	9.7	0.13
High-thrust	6.4	6.4	0.03	-1.5	-1.5	-0.05
Slowed-rotor	1.4	1.7	0.34	-6.7	-5.2	1.5

mately  $10^\circ$  of phase, but the shapes are otherwise very similar. Pitching moment predictions exhibit overprediction on the advancing side and underprediction on the retreating side. The pitching moment minimum in the second quadrant and the recovery in the third quadrant are not well represented. The dynamics for both normal force and pitching moment in the fourth quadrant arise from two dynamic stall cycles, one at  $\psi = 280^\circ$  and the second at  $\psi = 340^\circ$ . The CFD overpredicts the lift peaks preceding stall for both cycles. The moment pulses associated with these stall cycles are perfectly matched with the measured data in phase, but the magnitude of the pulses is overpredicted—especially for the second stall cycle.

Normal force for the slowed-rotor case (8737) is generally small and negative since this radial station was at a negative angle of attack for this test condition. Differences between measurement and prediction are also small and mostly characterized by underprediction of loading peaks. Pitching moment correlation displays a familiar overprediction on the advancing side and underprediction on the retreating side. Correlation of the minimum pitching moment in the second quadrant is particularly poor.

Individual sectional airloads are integrated to give global rotor performance indicators. Thrust and hub moments are among these but since they are trimmed quantities their comparison is uninteresting. Of the remaining performance metrics, rotor power and propulsive force are the most informative for these test conditions. These quantities are compared in Table 2. Rotor power coefficient is generally predicted within 4% for most test conditions. The exception is the slowed-rotor case where the magnitude of error is similar to the other conditions but is large relative to the low power value. The accuracy of predicted propulsive force is more mixed. This quantity is well predicted for the high-speed and high-thrust cases but the low-speed and slowed-rotor cases are poorly correlated with measurements.

Accurate prediction of rotor performance remains

a challenging problem for these simulations. For the purposes of the present study, accurate prediction of rotor torque coefficient (numerically equivalent to rotor power coefficient) is the most critical since it directly influences blade lag motion. Rotor propulsive force, although an important performance metric, has little bearing on blade motion.

## JOINT MOTION

The importance of hub articulation in improving rotor controllability and durability was realized early on in the evolution of the helicopter. The UH-60 aircraft has benefited from decades of articulated rotor design in the realization of its own rotor system. Each blade of the UH-60 rotor is retained by an elastomeric bearing. The focal point of the bearing acts as a hinge that allows the blade pitch, flap, and lag motion in exchange for reduced oscillatory hub loading. The displacement of these “hinges” from their neutral position is the primary measurement of the BMH and one component of the BD measurements. The CAMRAD II structural model for the UH-60 also simulates these hinges and can output hinge rotation predictions from the coupled simulations.

## PITCH

Changing blade pitch is the primary means of control for all helicopters. A constant pitch change is called collective and provides for control over the mean thrust of the rotor. Pitch changes that vary sinusoidally around the rotor azimuth are called cyclic and are a means to tilt the thrust vector and effect moments on the rotor hub. Cyclic can be expressed as the separate contributions of a sine and cosine function to the pitch. The portion associated with the cosine function is called lateral cyclic and provides rolling moments to the hub, while the sine component is called longitudinal cyclic and delivers pitching moments to the hub.

Figure 7 compares measured and predicted blade pitch motion versus azimuth for the four selected test conditions. The dominant  $1/rev$  pitch oscillation associ-

ated with cyclic is evident, and the collective input is visible as the mean pitch angle over one revolution. The large difference in collective between the low-speed case (Fig. 7a) and high-speed case (Fig. 7b) may seem surprising given that the rotor was producing approximately the same thrust for each case. However, the high-speed case required approximately  $9^\circ$  more forward shaft tilt to produce the additional propulsive force associated with high-speed flight. This increases the inflow to the rotor disk and therefore requires more collective pitch to produce the same amount of thrust. A similar situation is evident when comparing the high-speed case and the high-thrust case (Fig. 7c) where the collective difference is much smaller than expected given that the thrust differs by nearly a factor of two. Again, a large shaft angle difference between the two cases necessitates the high collective for the high-speed case. For the slowed-rotor case the collective was fixed at zero and this is reflected in Fig. 7d. The  $1/rev$  components of Fig. 7a-c are dominated by longitudinal cyclic which is necessary to achieve the prescribed pitching moments. The predominantly lateral cyclic visible in Fig. 7d was necessary to minimize  $1/rev$  flapping.

The two measurements, one from the BMH (crabarm) and one from the BD (photogrammetry), are in good agreement across all test conditions. The maximum deviation between the two curves is approximately  $1^\circ$ . The predictions exhibit larger deviations from the measured curves and those deviations vary with test condition. The minimally loaded slowed-rotor case correlates the best, with little difference between measurement and analysis beyond a small longitudinal cyclic input missed by the simulation. Next best is the low-speed case where there is a nearly constant  $1^\circ$  separation between the measured and predicted curves. This indicates that the analysis correctly predicted cyclic but overpredicted collective by approximately  $1^\circ$ . Predictions for the high-speed and high-thrust cases exhibit the most error. The maximum error is approximately  $3^\circ$  in both cases. Furthermore, the fact that error varies with azimuth indicates that the analysis has mispredicted both collective and cyclic. Quantifying the collective error is simply a matter of subtracting the means of both curves and this reveals a prediction error of  $2.1^\circ$  for both cases. Cyclic error is best quantified in polar form with the magnitude representing degrees of pitch and the phase representing degrees of azimuth. The predictions have a phase lead of approximately  $8^\circ$  for the high-thrust case and  $15^\circ$  for the high-speed case. Cyclic magnitude error is approximately  $0.75^\circ$  for the high-thrust case and  $0.50^\circ$  for the high-speed case. Some frequency content

greater than  $1/rev$  is present in the measurements but the analysis does not contain any significant harmonics above  $1/rev$ .

There are many sources of error possible in both the predictions and the measurements. All of the blade motion measurements are currently under review for sources of error and are still considered preliminary. On the prediction side, blade pitch motion is primarily determined by the CRA's trim algorithm interacting with the aerodynamics supplied by CFD. Any inaccuracy in the CFD solver that changes the relationship between blade pitch and blade loading would cause the predicted trim solution to deviate from truth. Turbulence modeling, transition modeling, and grid density are the usual suspects here, and exploring these avenues will be a topic of future work. In addition, the coupling process itself can be a source of error. Romander [4] described the effects of incomplete force conservation in coupled simulations. Any force "lost" in the communication between the CFD code and the CRA code will cause the CRA code to add additional collective or cyclic to make up for the missing force. Although the CRA model of the UH-60 used for this study incorporated all of the modifications suggested in [4], there is still a thrust disparity of as much as 1% between CFD and CRA for some of these conditions.

## FLAP

Out-of-plane motion by a blade as it travels around the azimuth is called flapping motion. It is this motion that allows the rotor tip-path-plane to deviate from the hub plane. The mean flapping angle is called coning and is principally determined by the thrust level. The sine and cosine components of  $1/rev$  flapping are called lateral and longitudinal flapping respectively. They are controlled by the corresponding lateral and longitudinal cyclic pitch inputs.

Measured and predicted flap angles are compared for a single rotor revolution at each test condition in Fig. 8. The coning angle clearly follows thrust: being identical between the high- and low-speed cases, at maximum for the high-thrust case, and at minimum for the zero collective slowed-rotor case. The low-speed case is the simplest example of  $1/rev$  flapping, consisting of almost pure longitudinal flapping that tilts the tip-path-plane forward. Figure 8b-d contain increasing levels of  $2/rev$  and  $3/rev$  flapping, a phenomena closely associated with increasing advance ratio.

Agreement between both measurements and predictions is generally very good for the low-speed, high-speed, and high-thrust cases. The prediction does show

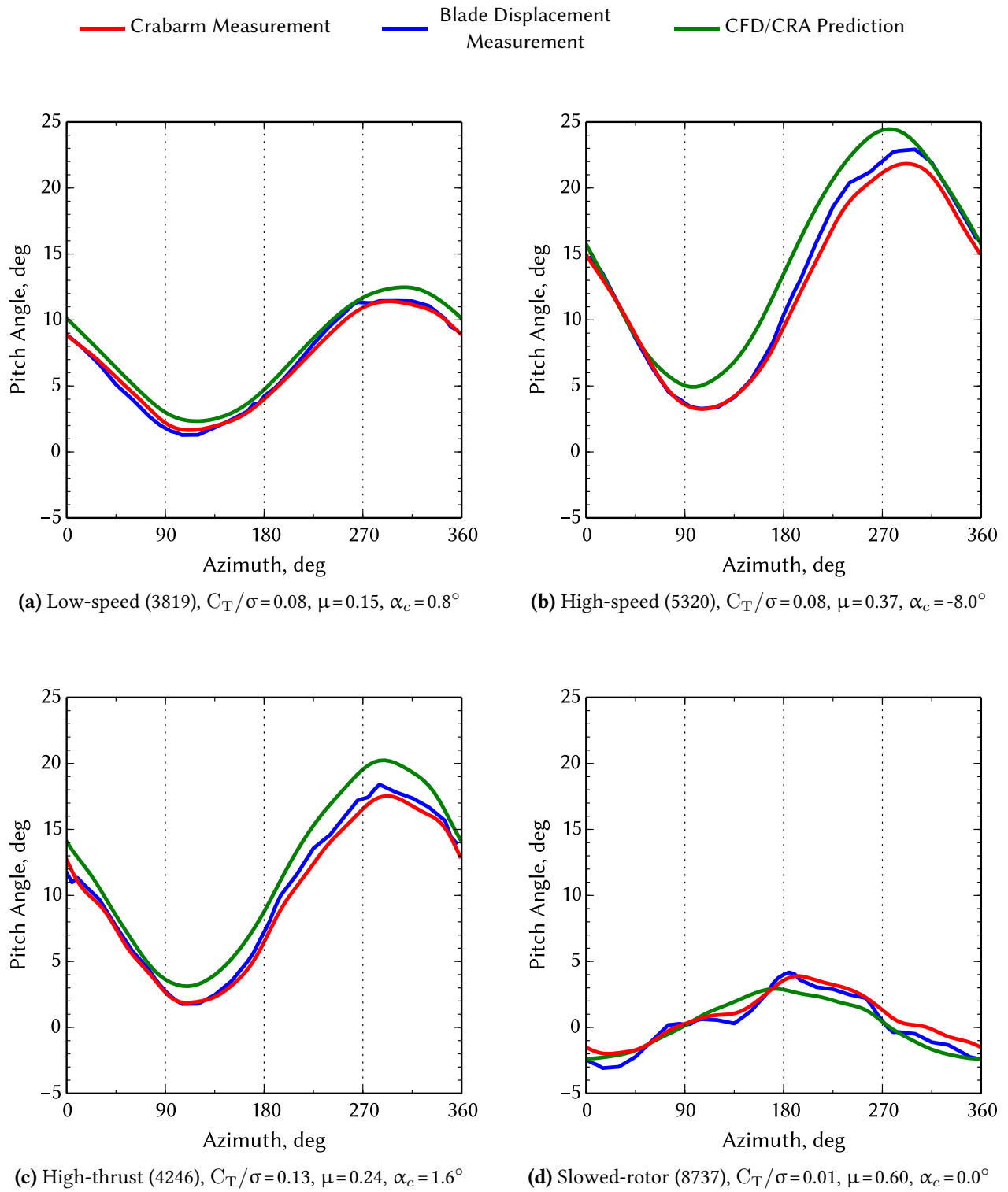


**Figure 7** – Pitch motion comparison at selected test conditions.

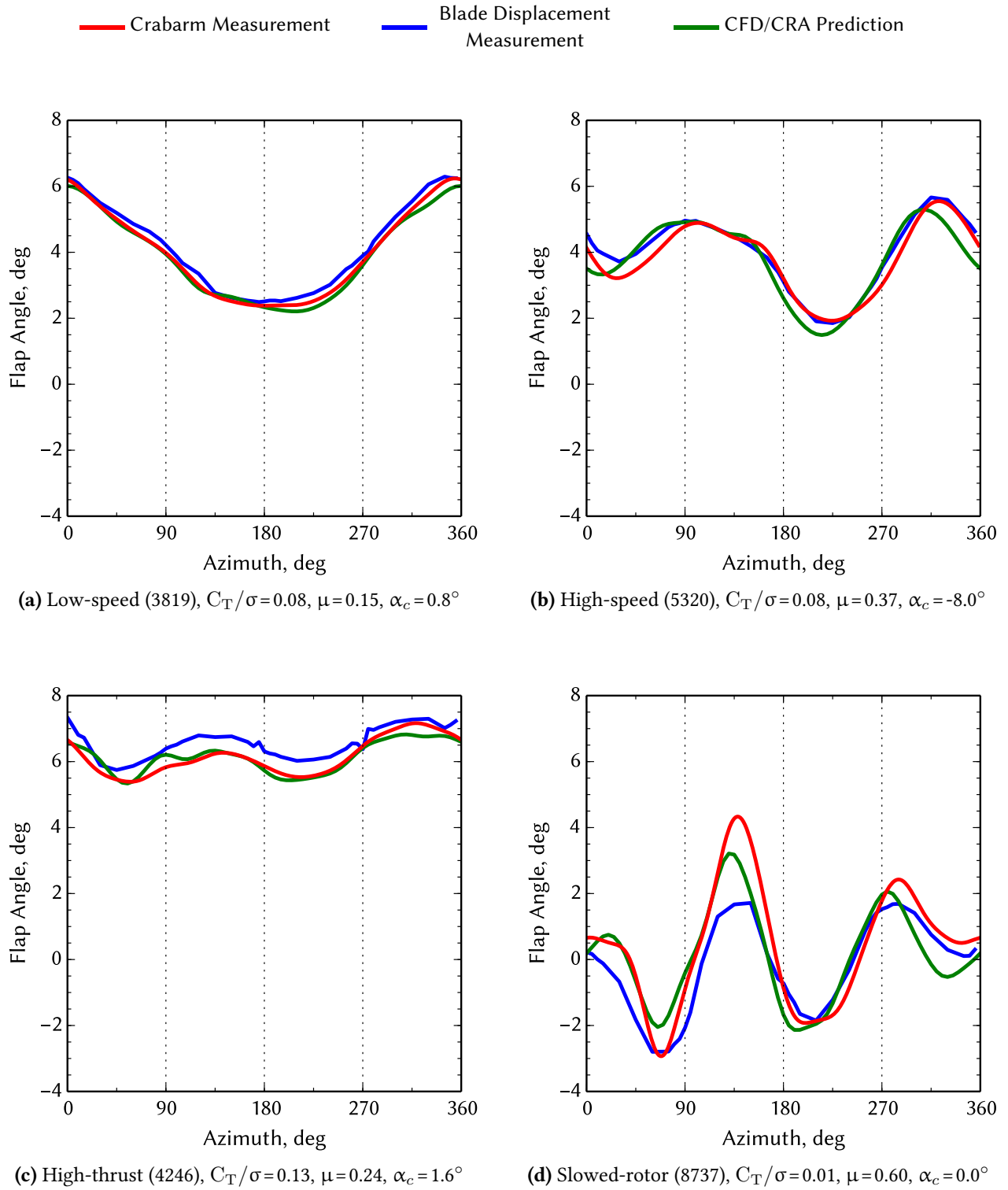


**Figure 8** – Flap motion comparison at selected test conditions.

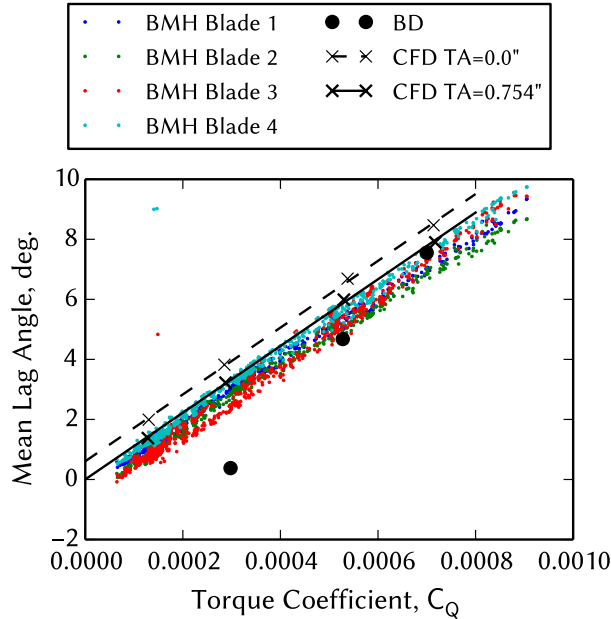


Figure 9 – Mean lag comparison.

approximately  $25^\circ$  of phase lead in the high-speed case which is consistent with the phase lead of predicted pitch motion. The BD measurement includes an additional  $1.5^\circ$  of coning compared to BMH and prediction for the high-thrust case. For the slowed-rotor case, the  $\frac{2}{\text{rev}}$  harmonic for the prediction leads the measurements by about  $25^\circ$  in phase while the amplitude is roughly between the measurements.

## LAG

Lead-lag motion (henceforth just “lag” motion) is the in-plane movement of a blade. This motion allows the rotor to dissipate energy from drag and Coriolis forces as the rotor turns. Because fluctuations in these forces are small when compared to the centrifugal force that stiffens lag motion, lag motion is often characterized by small oscillations about a larger mean.

Variation of mean lag with rotor torque exhibits a strong linear relationship. This line should pass near the origin since Coriolis forces have a zero mean value and no torque implies there are no in-plane forces to excite lag motion. Furthermore, the slope of the line is determined by the rate of rotation (which determines the magnitude of the centrifugal force) and various physical properties of the blade itself. Figure 9 plots BMH measured mean lag versus torque coefficient for each of the four blades at 903 different test points at nominal RPM. The validity of this linear relationship is clear despite

the wide variety of operating conditions. The consistency of slope from one blade to another indicates that the blades are physically similar. Also on Fig. 9 are three measurements of mean lag from the BD technique. The large difference in slope here suggests that this measurement provides an unreliable mean value of lag at present. The cause of this discrepancy is currently under investigation.

Four preliminary predictions of mean lag are fit by the dashed line in Fig. 9. Here a full RPM case at similarly low torque has been substituted for the slowed-rotor case since the reduced RPM would put it on a different line. These predictions match the slope of the BMH measured data very well but are offset from the origin by  $0.6^\circ$  of lag. Initial attempts to nullify this offset involved shifting the blade’s chordwise center of gravity and increasing the torque offset. The required shift to either of these model parameters was much larger than the accuracy to which they have been measured so these avenues were abandoned. Another option was to manipulate the location of the tension center—an unmeasured quantity assumed to lie on the elastic axis of the blade. Predictions using a constant tension center offset 0.754 inches away from the elastic axis in the direction of the trailing edge are shown fit with a solid line in Fig. 9. This tension center location results in the analysis predicting zero lag at zero torque but falls short of providing a best fit to the measured data. Relocating the tension center does have consequences for other aspects of the simulation—particularly structural loads—which have not been considered for the present work. Because the measured data is preliminary and a more comprehensive investigation was not performed, the tension center was not further adjusted in order to better fit the measurements.

Lag angle is plotted against azimuth in Fig. 10 for the four primary test conditions. As expected, the mean of each curve is proportional to torque and the oscillatory motion is small. Except for the mean shift, the BD measurement closely resembles the BMH measurement in character. The prediction captures the oscillatory components of the lag motion nicely but still overpredicts the BMH mean value slightly. Part of this error is due to the fact that the tension center shift was limited to intercepting the origin in Fig. 9, and this falls short of a tension center location that best fits the BMH data. A portion of this mean error is also due to the fact that the analysis mispredicts the mean torque by a few percent at each test condition (see Table 2).

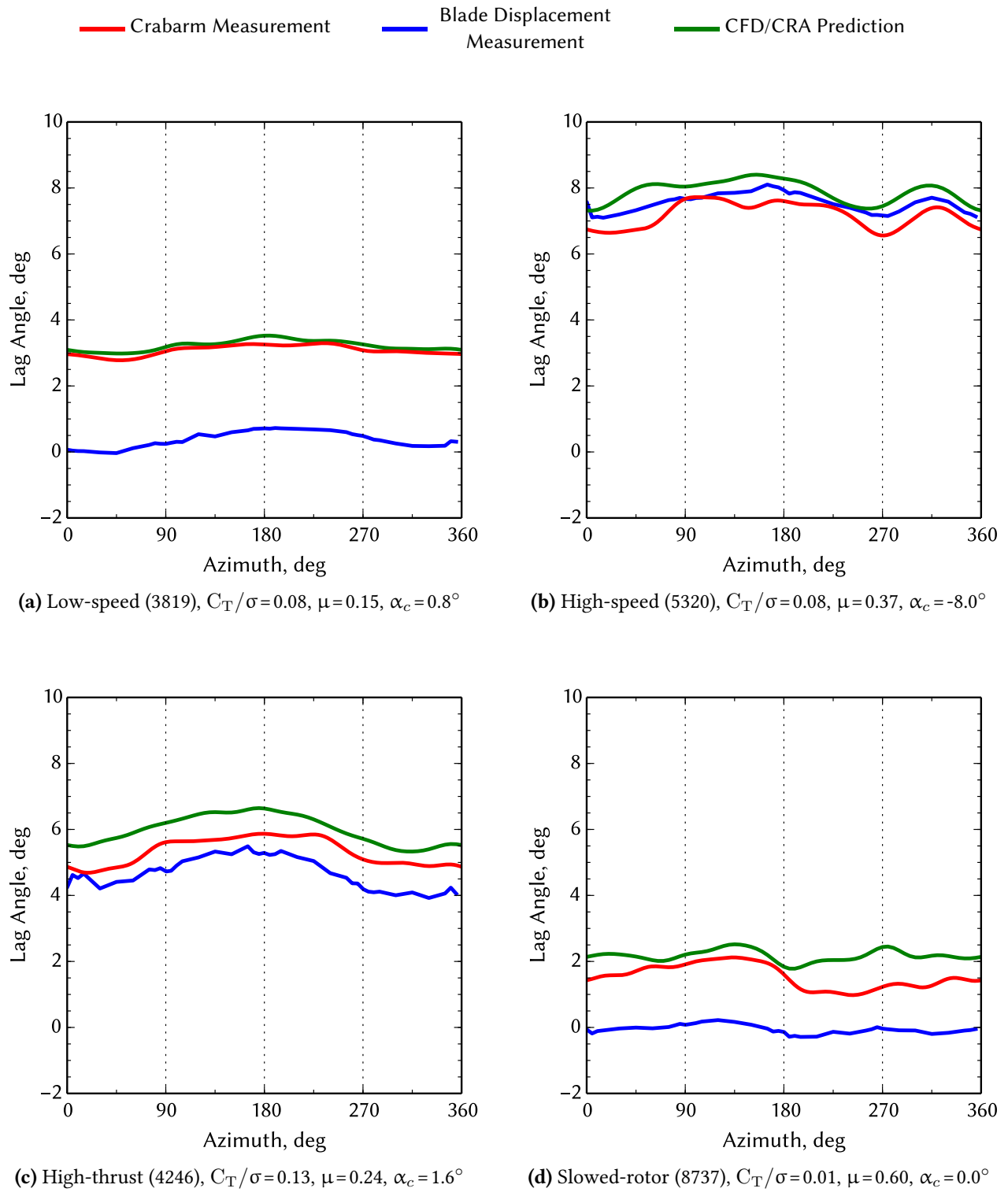


**Figure 10** – Lag motion comparison at selected test conditions.

## ELASTIC DEFORMATION

For a completely rigid blade, rotations about the three hub joints would be sufficient to comprehensively describe blade motion. However the thin, high aspect ratio blades of the UH-60 have considerable capacity to deform elastically. While it is possible to infer elastic deformation from strain gauge measurements taken on the surface of some blades, the BD measurement provides a more direct route to determine blade deformation.

The three primary elastic modes of a rotor blade are out-of-plane (flap) bending, torsion (twist deformation), and in-plane (chord) bending. Flap bending and torsion result in the largest displacements. Chordwise bending is small enough that its accurate measurement with the BD technique is currently uncertain and therefore no results for this mode will be presented.

Neither the BD measurement nor the analysis directly indicates elastic displacement. Rather, both give the total displacement of the blade from a rotating axis system centered on the hub. This displacement is the superposition of displacement due to hinge rotation and displacement due to elastic deformation. Because the hinge motions are known they are easily subtracted leaving only the elastic deformation, but this does mean that any error in the determination of the hinge motion will pollute the elastic deformation measurements.

Both the analysis and the BD measurement provide spanwise as well as azimuthal distributions of elastic deformation. For this paper correlation is performed versus azimuth at the blade tip because bending accumulates along the blade span. The tip therefore typically experiences the maximum deflection and should also exhibit maximum error.

## FLAP BENDING

Flap bending displacement at the blade tip is plotted against azimuth for the four test conditions in Fig. 11. The displacement is presented in inches measured relative to an infinitely rigid blade with the same flap hinge rotation.

For all four test conditions the mean bending at the tip is small and negative. The harmonic content at each test condition is very reminiscent of that presented for blade flap angle in Fig. 8. This is not surprising given that blade flapping and flap bending are both governed by the same forces. The phasing of the flap bending curves is very different between Fig. 11 and Fig. 8 however. This is due to the fact that motion at the flap hinge is primarily due to the first beam mode while flap bending is largely a consequence of the second beam mode.

Since the second beam mode moves the free end of the blade in the opposite direction from the first beam mode, the two curves go  $180^\circ$  out of phase.

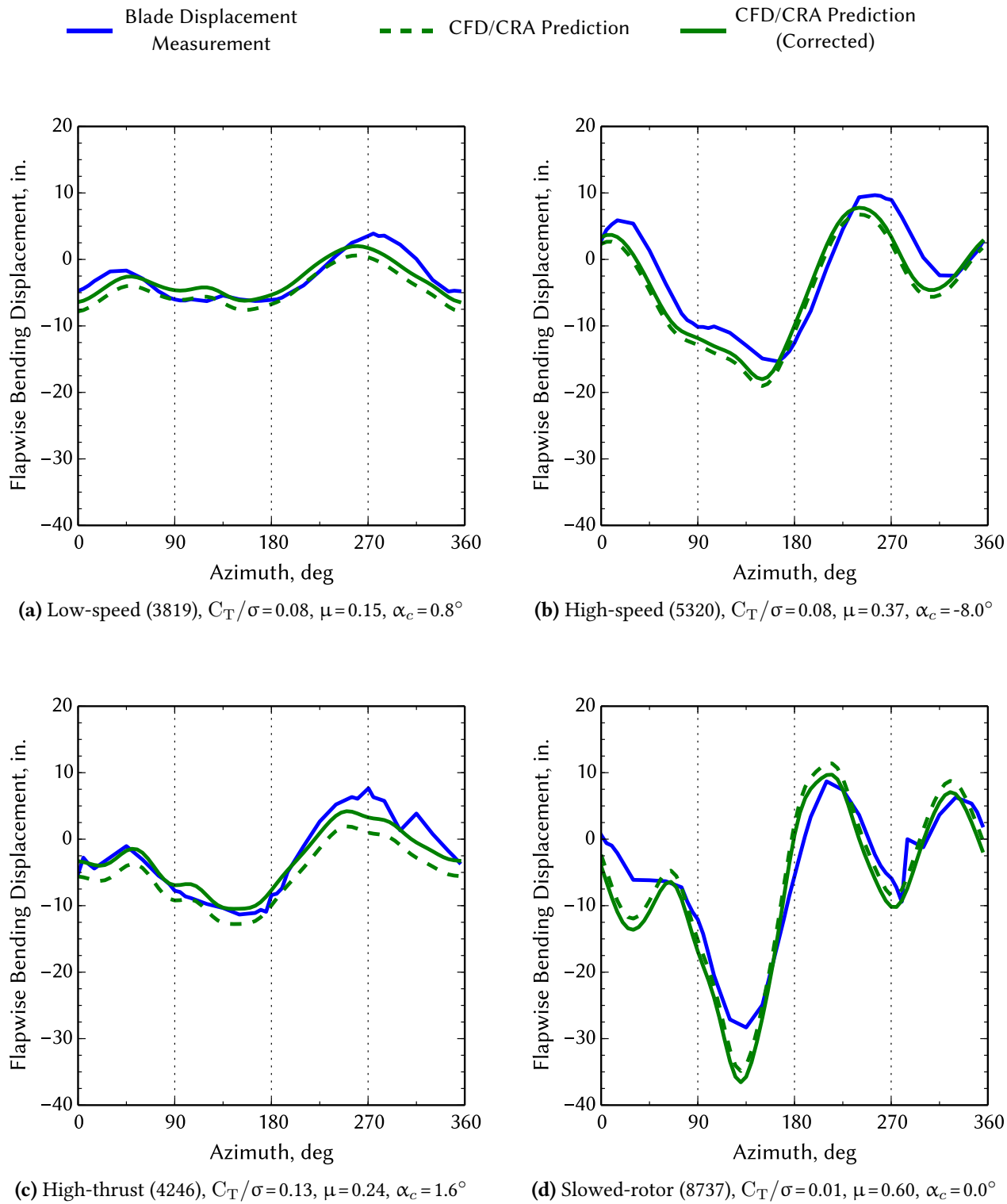
One degree of rotation at the flap hinge results in 5 inches of travel at the blade tip, and error in flap angle for both measurements and predictions feeds into flap bending at this rate. For this reason, two curves are presented for the analysis: the dashed curve is the raw predicted displacement while the solid curve has been corrected for differences in mean flap hinge rotation. The correction is generally small since the mean flap angle is well predicted by the analysis (Fig. 8). Some of the remaining differences between measured and predicted flap bending can be related to differences in flap angle prediction in Fig. 8. These differences include the phase shift at high-speed and the error in predicting some of the peaks for the slowed-rotor case. Differences in the 4<sup>th</sup> quadrant for the low-speed and high-thrust cases, however, do not appear to have origins in flap angle mispredictions.

Conspicuously absent from Fig. 8 and Fig. 11 is any motion in response to the high-frequency loading of BVI or dynamic stall for the low-speed or high-thrust cases. The magnitude of the normal force fluctuation due to BVI (Fig. 6a), in particular, seems large enough to provoke a response from the blade. However, the frequency of the loading is simply too high for the blades to respond with motion. Instead this loading is transferred to the hub where it is either absorbed by the structure or passed on to the aircraft.

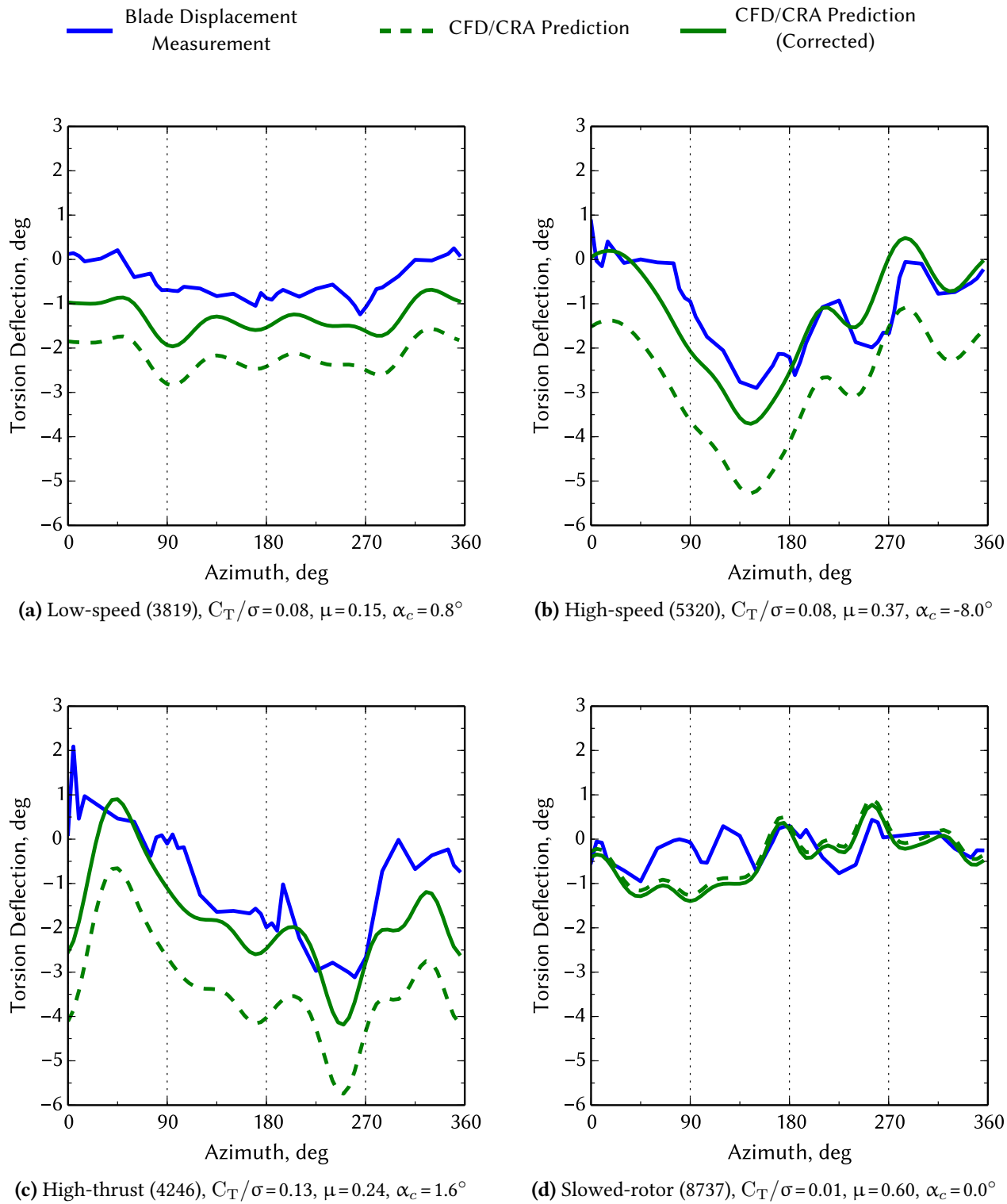
## TORSION

Figure 12 presents torsion deflection for each of the considered test conditions. The analysis data is again plotted both uncorrected and also with a correction for mean pitch angle from Fig. 7. The correction in this case arises from the analysis' failure to correctly predict the collective required to meet the specified thrust target.

The means are again consistently small and negative for each test condition. The curves contain a visible  $5/\text{rev}$  component which is consistent with the torsional natural frequency of this rotor. This displacement is more difficult for the BD technique to accurately compute because the position error is larger relative to the chordwise separation of targets than it is to the spanwise separation. Thus it is nearly certain that the very high frequency oscillations (e.g. the excursion near  $\psi=0^\circ$  for the high-thrust case) are non-physical. The corrected predictions are well matched to the BD measurements. Mean shifts of approximately  $1^\circ$  are present for the low-speed and high-thrust cases.



**Figure 11** – Flapwise bending comparison at  $r/R=0.97$  for selected test conditions.



**Figure 12** – Torsion comparison at  $r/R=0.97$  for selected test conditions.

The slowed-rotor case shows some  $1/rev$  oscillation not present in the measurement but this is really a consequence of the analysis failing to predict—and therefore remove—the slight longitudinal cyclic input present in Fig. 7d. The high-speed case exhibits a small phase lead also due to mispredicted cyclic in Fig. 7b.

Again the blade appears indifferent to the high frequency loads shown in Fig. 6. The pitching moment pulses caused by dynamic stall (e.g. Fig. 6c) are a known design problem for rotors that might experience stall. These pulses are too evanescent to be absorbed by the blade through torsion and so they are transferred to the pitch links where they have important consequences for structural design.

## SUMMARY

The recently completed UH-60A Airloads wind tunnel test included multiple measurements of blade motion. One mechanical system and one laser system measured pitch, flap, and lag angles for each blade. In addition, a novel system based on photogrammetry captured bulk blade motion including deformation. This paper is an initial attempt to comprehensively survey these measurements and correlate them with high fidelity simulation.

The simulation package included a Comprehensive Rotorcraft Analysis package, CAMRAD II, augmented with the first principles aerodynamics of a CFD simulation provided by OVERFLOW 2. Four very different test conditions were modeled: a low-speed case featuring multiple blade-vortex interactions, a high-speed case, a high-thrust case with the rotor deeply stalled, and a slowed-rotor case at high advance ratio.

Pitch bearing rotations are dominated by control inputs required to trim the rotor. Here the analysis displayed a tendency to overpredict collective and cyclic magnitudes by a small amount. In addition, a modest phase lead is present in the predicted cyclic for the high-speed and slowed-rotor cases. This phase lead propagated through the simulation and is observable in other blade motion predictions as well. Two factors are suspected in the misprediction of the trim state and both are related to aerodynamics. The first is simple error in the CFD simulation which causes the blade to produce less lift for a given collective than it should. The second is incomplete force conservation in the transfer of forces from CFD to CRA. These “lost” forces must be compensated for by increased control inputs.

Flap angle prediction accuracy is generally on the order of  $1^\circ$  which suggests that the out-of-plane load dis-

tribution provided by CFD is reasonable, that the simplified structural model of the blade is adequate, and that the relevant physical properties of the blade have been accurately measured. The only exception is the slowed-rotor case where there are differences of  $1-2^\circ$  between the two measurements themselves as well as differences of up to  $1^\circ$  between each measurement and the analysis.

Initial efforts to predict lag motion were unsuccessful at accurately capturing the mean value. An analysis of the predicted mean lag variation with rotor torque revealed that although most of the model blade’s physical properties are correct, one or more of the torque offset, chordwise CG, or tension center location is likely causing a mean shift in the predicted lag motion. Based on engineering judgment, the tension center was moved a constant 0.754 inches aft from the elastic axis while the torque offset and CG location were held constant. This moved mean lag to within  $1^\circ$  of the measured data for the selected test conditions. This same analysis also revealed that the mean lag value measured by the BD process is highly suspect. Oscillatory components of lag are small but appear to be in good agreement between the simulation and both measurements.

Data from two blade elastic modes has also been correlated between the BD measurement and simulation. Extraction of bending data is complicated by error in motion at the associated hub hinge. Part of this can be accounted for by correcting the mean value of the predicted deflection to account for error in the mean value of the associated hinge rotation.

Flap bending, like flap hinge rotation, is well predicted by the analysis. The prediction deviates from the measurement by as much as 5 inches of deflection but this equates to less than one degree of flap hinge rotation. Many of the deviations can be traced to incorrect flap angle predictions (and therefore all the way back to mispredictions of pitch angle in some cases).

Torsion was likewise investigated. Here the BD measurement begins to approach its accuracy limits due to the chordwise separation of targets but the data remains useful. Shifting the mean value of the predictions significantly improves correlation for torsion. A few additional discrepancies can be traced back to mispredicted pitch bearing rotation. The remaining error is on the order of  $1^\circ$ .

## REFERENCES

- [1] Lorber, P.F., “Aerodynamic Results of a Pressure-Instrumented Model Rotor Test at the DNW”, *Jour-*

- nal of the American Helicopter Society*, Vol. 36, No. 4, October 1991.
- [2] Kufeld, R.M., Balough, D.L., Cross, J.L., Studebaker, K.F., Jennison, C.D., and Bousman, W.G., "Flight Testing of the UH-60A Airloads Aircraft", American Helicopter Society 50<sup>th</sup> Annual Forum, Washington, D.C., May 1994.
- [3] Norman, T.R., Shinoda, P., Peterson, R.L., and Datta, A., "Full-Scale Wind Tunnel Test of the UH-60A Airloads Rotor", American Helicopter Society 67<sup>th</sup> Annual Forum, May 2011.
- [4] Romander, E., Norman, T.R., and Chang, I-C., "Correlating CFD Simulation With Wind Tunnel Test for the Full-Scale UH-60A Airloads Rotor", American Helicopter Society 67<sup>th</sup> Annual Forum, May 2011.
- [5] Lee-Rausch, E.M. and Biedron, R.T., "FUN3D Airload Predictions for the Full-Scale UH-60A Airloads Rotor in a Wind Tunnel", American Helicopter Society 69<sup>th</sup> Annual Forum, May 2013.
- [6] Potsdam, M., Datta, A., and Jayaraman, B., "Computational Investigation and Fundamental Understanding of a Slowed UH-60A Rotor at High Advance Ratio", American Helicopter Society 68<sup>th</sup> Annual Forum, May 2012.
- [7] Yeo, H. and Romander, E.A., "Loads Correlation of a Full-Scale UH-60A Airloads Rotor in a Wind Tunnel", *Journal of the American Helicopter Society*, Vol. 58, No. 2, April 2013.
- [8] Ahmad, J.U., Yamauchi, G.K., and Kao, D.L., "Comparison of Computed and Measured Vortex Evolution for a UH-60A Rotor in Forward Flight", AIAA-2013-3160, 31<sup>st</sup> American Institute of Aeronautics and Astronautics Applied Aerodynamics Conference, June 2013.
- [9] Abrego, A.I., Olson, L.E., Romander, E.A., Barrows, D.A., and Burner, A.W., "Blade Displacement Measurement Technique Applied to a Full-Scale Rotor Test", American Helicopter Society 68<sup>th</sup> Annual Forum, May 2012.
- [10] Buning, P.G., Gomez, R.J., and Scallion, W.I., "CFD Approaches for Simulation of Wing-Body Stage Separation", AIAA-2004-4838, AIAA 22<sup>nd</sup> Applied Aerodynamics Conference, Providence, RI, August 16-19, 2004.
- [11] Potsdam, M., Strawn, R.C., and Meakin, R., "Dynamic Rotorcraft Applications Using Overset Grids", 31<sup>st</sup> European Rotorcraft Forum, Florence, Italy, September 13-15, 2005.
- [12] Spalart, P.R., Jou, W-H., Strelets, M. and Allmaras, S.R., "Comments on the Feasibility of LES for Wings and on a Hybrid RANS/LES Approach", First AFOSR Conference on DNS/LES, August 1997, Greyden Press, Columbus, OH.
- [13] Johnson, W., "Technology Drivers in the Development of CAMRAD II", American Helicopter Society Aeromechanics Specialist Meeting, San Francisco, CA, January 19-21, 1994.
- [14] Yeo, H., Bousman, W.G., and Johnson, W., "Performance Analysis of a Utility Helicopter with Standard and Advanced Rotor", *Journal of the American Helicopter Society*, Vol. 49, No. 3, July 2004, pp. 250-270.
- [15] Shinoda, P.M., Yeo, H., and Norman, T.R., "Rotor Performance of a UH-60 Rotor System in the NASA Ames 80- by 120-Foot Wind Tunnel", *Journal of the American Helicopter Society*, Vol. 49, No. 4, October 2004.
- [16] Yeo, H., and Johnson, W., "Assessment of Comprehensive Analysis Calculation of Airloads on Helicopter Rotors", *Journal of Aircraft*, Vol. 42, No. 5, September-October 2005.
- [17] Yeo, H., and Johnson, W., "Prediction of Rotor Structural Loads with Comprehensive Analysis", *Journal of the American Helicopter Society*, Vol. 53, No. 2, April 2008.
- [18] Yeo, H., Romander, E., and Norman, T., "Investigation of Rotor Performance and Loads of a UH-60A Individual Blade Control System", American Helicopter Society 66<sup>th</sup> Annual Forum, Phoenix, AZ, May 11-13, 2010.
- [19] Tung, C., Caradonna, F.X., and Johnson, W., "The Prediction of Transonic Flows on an Advancing Rotor", American Helicopter Society 40<sup>th</sup> Annual Forum, Arlington, VA, May 16-18, 1984.
- [20] Potsdam, M., Yeo, H., and Johnson, W., "Rotor Airloads Prediction Using Loose Aerodynamic/Structural Coupling", *Journal of Aircraft*, Vol. 43, No. 3, May-June 2006.

- [21] Nygaard, T., Saberi, H., Ormiston, R.A., Strawn, R.C., and Potsdam, M., "CFD and CSD Coupling Algorithms and Fluid Structure Interface for Rotorcraft Aeromechanics in Steady and Transient Flight Conditions", American Helicopter Society 62<sup>nd</sup> Annual Forum, Phoenix, AZ, May 9–11, 2006.
- [22] Langer, H.J., Peterson, R.L., and Maier, T.H., "An Experimental Evaluation of Wind Tunnel Wall Correction Methods for Helicopter Performance", American Helicopter Society 52<sup>nd</sup> Annual Forum, Washington, D.C., June 1996.